Japanese Journal of Radiology (2019) 37:109–116
https://doi.org/10.1007/s11604-018-0787-3

INVITED REVIEW

# Amide proton transfer imaging of tumors: theory, clinical applications, pitfalls, and future directions

**Kiyohisa Kamimura[1] · Masanori Nakajo[1] · Tomohide Yoneyama[1] · Koji Takumi[1] · Yuichi Kumagae[1] · Yoshihiko Fukukura[1] · Takashi Yoshiura[1]**

Received: 16 August 2018 / Accepted: 10 October 2018 / Published online: 19 October 2018


**Abstract**
Amide proton transfer (APT) imaging is an emerging molecular magnetic resonance imaging technique based on chemical exchange saturation transfer (CEST). APT imaging has shown promise in oncologic imaging, especially in the imaging of brain tumors. This review article illustrates the theory of CEST/APT imaging and describes the clinical utility, pitfalls, and potential for future development of APT imaging.

**Keywords** Amide proton transfer · Chemical exchange saturation transfer · Tumor

## Introduction

Histopathological examination has been considered the gold standard for the diagnosis of tumors, and molecular and genetic information has become increasingly incorporated into this diagnostic approach [1]. However, in clinical settings, non-invasive imaging diagnosis greatly contributes to every aspect of management. Magnetic resonance (MR) imaging plays a particularly important role in diagnosing central nervous system (CNS) tumors, as it provides higher lesion-to-normal contrast than computed tomography. Conventional MR imaging techniques, such as T2-weighted imaging, fluid-attenuated inversion recovery (FLAIR) imaging, and contrast-enhanced T1-weighted imaging, offer important information for characterizing tumors. Moreover, quantitative imaging biomarkers derived from advanced MR imaging techniques, such as diffusion-weighted imaging and perfusion imaging, have proven useful in further characterizing tumors on the basis of microstructure and vascularization [2–5]. Nevertheless, these methods have sometimes resulted in conflicting results or overlap in measured values. Thus, new imaging methods with greater specificity to tumor biology are desired.

✉ Kiyohisa Kamimura
kiyohisa@m2.kufm.kagoshima-u.ac.jp

[1] Department of Radiology, Kagoshima University Graduate School of Medical and Dental Sciences, 8-35-1 Sakuragaoka, Kagoshima 890-8544, Japan

Chemical exchange saturation transfer (CEST) is a novel MR imaging contrast technique that relies on the molecular characteristics of the sample [6]. Amide proton transfer (APT) imaging is an emerging CEST-based MR imaging technique [7] that is sensitive to mobile proteins and peptides in the tissue. APT imaging has become increasingly recognized as a promising imaging modality for tumors. This review article illustrates the fundamental principles of CEST and APT, describes the utility and pitfalls of APT imaging in oncology, and finally discusses future directions for its application.

## Theory of CEST and APT

Figure 1 illustrates the basic principle of CEST. CEST is based on the transfer of saturation between solute molecules and water molecules via chemical exchange; in this transfer, a proton physically moves back and forth between the solute and the solvent (water). The solute proton has a resonance frequency different from that of water but is invisible with conventional MR imaging because of the very low solute concentration (typically on the order of millimolar). The exchangeable protons of the solute are saturated via a selective saturation radio frequency (RF) pulse at the solute frequency. The saturation is transferred to the bulk water via chemical exchange, thereby decreasing the magnetization and signal of the water. The saturation transfer continues during irradiation by the saturation pulse, resulting in a build-up of saturation in the bulk water pool. This

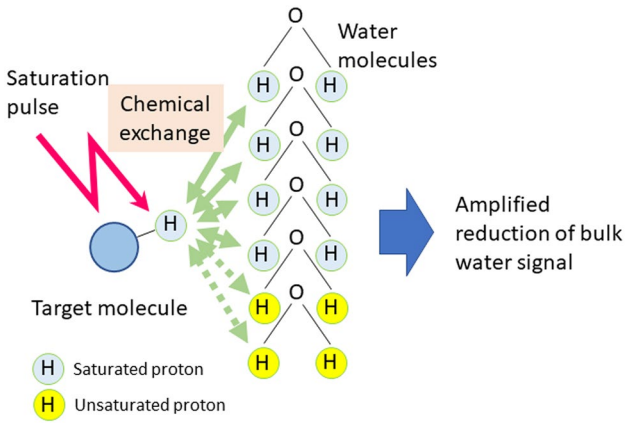


**Fig. 1** Schematic of the principle behind CEST. Exchangeable protons of solute molecules are saturated with a specific saturation pulse. The saturated protons are transferred to water molecules via chemical exchange. Continuous irradiation of the saturation pulse results in the build-up of saturation in the water molecules, thus amplifying the bulk water signal reduction

amplification mechanism allows for the indirect observation of low-concentration solutes.

Figure 2 shows the Z-spectrum, which is a plot of the bulk water signal intensity against different saturation pulse offset frequencies. The water signal is strongly suppressed at 0 ppm, which is the water resonance frequency, because of direct saturation. The CEST effect is usually observed as a small dip in the spectrum at the specific frequency of the solute protons.

The proton exchange rate must be slow enough to enable the selective saturation of the solute protons but fast enough to induce a detectable water signal reduction. Generally in CEST, a higher magnetic field is advantageous, as the shift difference in hertz increases in proportion to the magnetic field strength. CEST experiments can be conducted using both endogenous and exogenous molecules. A number of exogenous CEST agents have been proposed for various specific purposes [8–10], but these are beyond the scope of this review.

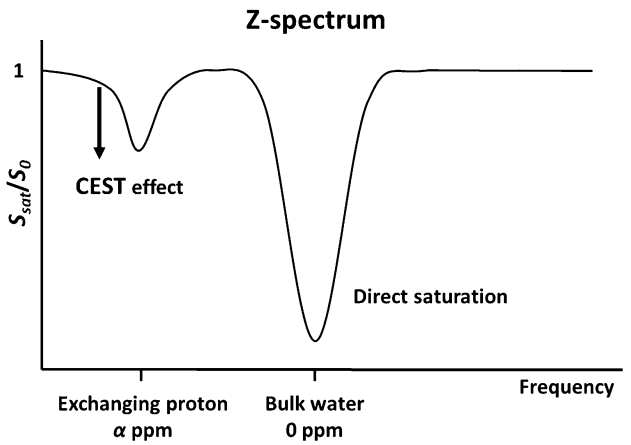


**Fig. 2** Z-spectrum. The signal intensity of bulk water is plotted at varying offset frequencies of the saturation pulse. A strong suppression due to direct saturation is present at the water resonance frequency (0 ppm). The CEST effect is observed as a smaller signal reduction at the specific frequency for the solute protons ($\alpha$ ppm)

The feasibility of endogenous CEST imaging was first demonstrated in the imaging of urea in the bladder of healthy human subjects [11]. Since then, several endogenous metabolites with exchangeable protons in amide (–NH), amine ($–NH_2$), and hydroxyl (–OH) groups with optimal exchange properties under physiological conditions have been identified and imaged in vivo (Table 1) [12–16]. Thus, CEST-based MR imaging shows promise as a non-invasive, non-ionizing tool for molecular imaging.

APT imaging is a specific type of endogenous CEST imaging technique proposed by Zhou et al. [7]. This method enables the semi-quantitative measurement of amide protons (–NH) in intrinsic mobile proteins and peptides, which have a specific resonance frequency 3.5 ppm downfield from that of water. Because this resonance frequency is sufficiently remote from that of water and amide protons are relatively abundant in tissue, especially in tumors, APT imaging is considered to be the most clinically relevant type of CEST imaging.

The amide proton transfer ratio (APTR), which is the exchange transfer effect per proton, has been described as [7]

$$\mathrm{APTR} = \frac{k\,[\text{amide proton}]}{2[\mathrm{H_2O}]R_{1\mathrm{w}}}(1 - \mathrm{e}^{-R_{1\mathrm{w}}t_{\mathrm{sat}}}),$$

where $k$ is the exchange rate constant, $R_{1\mathrm{w}}$ ($=1/T_{1\mathrm{w}}$) is the spin–lattice relaxation rate of water, and $t_{\mathrm{sat}}$ is the saturation time. As shown by this equation, the APT effect is dependent on not only the fractional concentration of exchangeable amide protons but also several other parameters, including the T1 of water, $T_{1\mathrm{w}}$, and the saturation pulse length $t_{\mathrm{sat}}$. It is also important to note that the proton exchange rate constant $k$ is dependent on physiological conditions such as the pH and temperature.

**Table 1** Types of CEST imaging

| Proton | CEST imaging |
|---|---|
| Amides proton (–NH) | Amide proton transfer (APT) |
| Amine proton ($–NH_2$) | Glutamate (GluCEST) |
| | Creatine (CrCEST) |
| Hydroxyl proton (–OH) | Glycogen (GlycoCEST) |
| | Myoinositol (MICEST) |
| | Glucose (GlucoCEST) |
| | Glycosaminoglycans (GagCEST) |

## APT imaging sequence

Pulse sequences in APT imaging include a saturation pulse followed by an image acquisition component. The saturation pulse is typically long (0.5–2 s), because a longer pulse will saturate more water protons [17]. To obtain the full spectrum of the water signal intensity, imaging is repeated with different saturation pulse frequencies.

Several sequences, such as two-dimensional (2D) fast spin-echo (FSE) [18], 2D gradient-echo (GE) [19], and 2D spin-echo echo-planar imaging (SE-EPI) [20], are used for image acquisition. 2D sequences evaluate only one slice of a tumor or require a long time to evaluate a whole tumor. Volume data acquisition is essential for clinical use to evaluate a whole tumor. Recently, three-dimensional (3D) volume data acquisition sequences, including sequences based on 3D FSE [21] and 3D gradient- and spin-echo (GRASE) [22], have become available.

The scanning time varies widely depending on the number of saturation pulse frequencies and slice levels. With a single-slice 2D FSE sequence obtaining the full spectrum, the scanning time may be approximately 3 min. A scan with a 3D sequence covering a large part of the brain may be finished in approximately 7–8 min if the choices of saturation pulse frequencies are limited to those specific for APT (i.e., around ± 3.5 ppm). In any case, an additional scan may be necessary for voxel-wise correction for $B_0$ inhomogeneity (see the next section).

## Measurement of APT effect

As described earlier, CEST imaging is based on the saturation of solute protons at their specific frequency. However, this process may be hampered by magnetic field inhomogeneities in the magnet, which in turn produce a shift in the Z-spectrum. Thus, correction for $B_0$ inhomogeneities in each voxel is essential for accurate measurement. Several different correction methods have been proposed; these include realigning the 0 ppm to the minima of the interpolated Z-spectrum [7]; a water suppression shift referencing (WASSR) method, in which direct water saturation is identified using low-power RF pulses [23]; and correction using a separately obtained $B_0$ map [24].

The Z-spectrum not only consists of direct saturation and the CEST (APT) effect but also includes signal reductions by the nonspecific magnetization transfer (MT) effect and the nuclear Overhauser effect (NOE). The nonspecific MT effect represents saturation transfer via complex mechanisms involving cross-relaxation [25] and chemical exchange [26]. In contrast to CEST, which is based on saturation transfer through proton exchange (chemical exchange) between water and mobile structures with long T2, nonspecific MT occurs between semisolid macromolecules with short T2, such as myelin and water. The NOE is another saturation transfer mechanism that is observed upfield from the water frequency [27].

The APT effect is most often quantified as the asymmetry of the MT ratio, $MTR_{asym}$, at 3.5 ppm, given as

$$MTR_{asym}(3.5\ \text{ppm}) = (S_{-3.5\text{ppm}} - S_{3.5\text{ppm}})/S_0,$$

where $S_{-3.5\text{ppm}}$ and $S_{3.5\text{ppm}}$ are the signal intensities at − 3.5 and 3.5 ppm, respectively, and $S_0$ is the unsaturated signal intensity.

This approach effectively eliminates the overlapping direct saturation and nonspecific MT effects because of their symmetric nature; however, the upfield NOE signal remains as a confounding factor in the quantification of downfield APT. Nevertheless, the $MTR_{asym}$ value at 3.5 ppm is widely accepted as an approximate index of the APT signal intensity and is often called APT-weighted signal intensity (APTWSI). APT-weighted images are obtained by performing the voxel-wise mapping of this index (Fig. 3) [7]. Several other approaches to obtain pure APT images have been recently proposed [28–30].

## Clinical applications to brain tumors

APT imaging selectively detects amide protons in mobile proteins and peptides. In contrast to semisolid structural proteins, mobile proteins are found mainly as cytosolic, endoplasmic reticulum, and secreted proteins. The underlying assumption in the APT imaging of tumors is that there is a close relationship between the proliferative activity of the tumor and mobile protein synthesis. Yan et al. [31] used rats implanted with gliosarcomas and showed that in comparison with healthy brain tissue, tumor tissue contains an

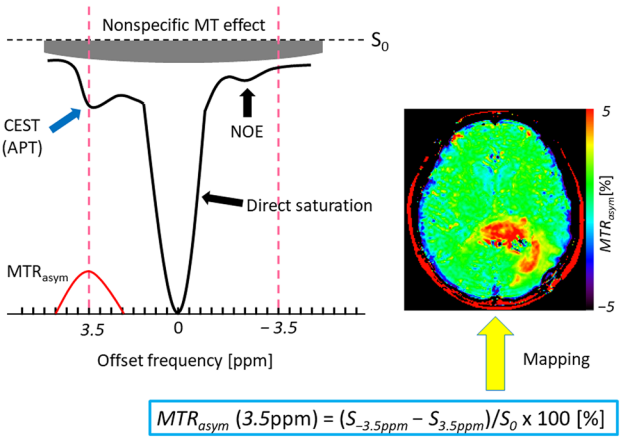


**Fig. 3** APT effect measured as $MTR_{asym}$ at 3.5 ppm, the asymmetry of the MT ratio at 3.5 ppm excluding contributions from symmetric direct saturation and the nonspecific MT effect. The NOE upfield of water remains a confounding factor. APT-weighted images are obtained via the voxel-by-voxel mapping of $MTR_{asym}$ at 3.5 ppm

increased concentration of cytosolic proteins that contribute to the APT signal despite there being virtually no difference between the total protein concentrations of the two tissues. Moreover, proteomic analyses have shown that there are different expressions between astrocytomas and normal brain tissues as well as among different grades of astrocytomas [32].

## Prediction of malignancy grade in diffuse gliomas

Discrimination between low- and high-grade gliomas is critical because the prognoses and thus appropriate therapeutic strategies differ substantially between these two cases in many tumors [33]. In previous studies, the APTWSI ($MTR_{asym}$ at 3.5 ppm) was found to be 3–4% higher in tumor tissue than in peritumoral brain tissue for human brain tumor at 3 T [34]. Moreover, the APTWSIs in six high-grade gliomas were found to be higher than those in three low-grade gliomas ($2.9 \pm 0.6\%$ vs. $1.2 \pm 0.2\%$) [34]. This preliminary result suggests the potential of APT imaging for grading gliomas based on this novel contrast mechanism in a clinical setting. Togao et al. [35] have reported a significant positive correlation between World Health Organization (WHO) grade and APTWSI in 36 adult diffuse gliomas, demonstrating the clinical utility of APT imaging in predicting the histological grade. In the report, APTSWI could differentiate high-grade (grade III and IV) gliomas from low-grade (grade II) ones with a sensitivity of 93% and a specificity of 100%. The same research group has shown that the APTWSI is superior to the apparent diffusion coefficient and relative cerebral blood volume in distinguishing malignant gliomas without intense contrast enhancement from benign gliomas [36]. The usefulness of the APTWSI in grading gliomas has been confirmed by several research groups [37, 38]. Figure 4 shows APT-weighted images of low- to high-grade gliomas.

## Prediction of genetic mutation in gliomas

In the recently revised WHO classification, gliomas are diagnosed based on a combination of histological findings and molecular information [1]. One of the most important genetic mutations in diffuse gliomas is the isocitrate dehydrogenase (IDH) mutation. This mutation has been implicated in oncogenesis in several types of tumors and is known to have a major impact on the prognosis of affected patients. That is, the presence of the IDH mutation is recognized as a marker of favorable prognosis in grade II and III astrocytomas and glioblastomas [39, 40]. Thus, preoperative detection of this mutation may help plan an appropriate therapeutic strategy.

Jiang et al. [41] investigated whether APT imaging is useful in noninvasively predicting the IDH mutation status in grade II gliomas. They reported that IDH-wildtype gliomas tended to have higher APTWSIs than IDH-mutant tumors (IDH-wildtype: $1.39 \pm 0.49\%$ vs. IDH-mutant: $0.93 \pm 0.44\%$), suggesting the predictive value of APT imaging.

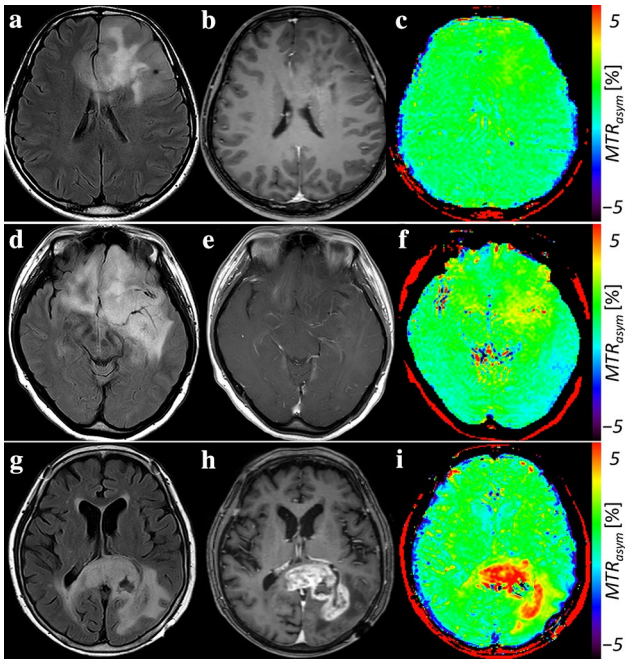


**Fig. 4** APT-weighted images of **a**–**c** grade II (oligodendroglioma), **d**–**f** grade III (anaplastic oligodendroglioma), and **g**–**i** grade IV (glioblastoma) gliomas. Note that the APTWSI was measured as the $MTR_{asym}$ value at 3.5 ppm increases with increasing grade

## Differentiation between malignant gliomas and malignant lymphomas

There have been few studies on utility of APT imaging in the differential diagnosis of brain tumors. Jiang et al. [42] have demonstrated the usefulness of APT imaging in differentiating high-grade gliomas from primary CNS malignant lymphomas (PCNSLs). In their report, PCNSLs had significantly lower maximum APTWSI ($APTW_{max}$) than high-grade gliomas ($3.38 \pm 1.06\%$ vs. $4.36 \pm 1.30\%$). This finding was hypothetically attributed to higher nucleus–cytoplasm ratios in PCNSLs, which would reduce the amount of cytoplasmic protein. Moreover, PCNSLs showed significantly lower differences between the maximum and minimum APTWSIs ($APTW_{max-min}$) than high-grade gliomas ($0.76 \pm 0.42\%$ vs. $2.55 \pm 1.20\%$), indicating a lower heterogeneity. The $APTW_{max-min}$ could differentiate the two tumor types with a sensitivity of 100% and a specificity of 84.6% [42]. Figure 5 shows examples of images of a PCNSL.

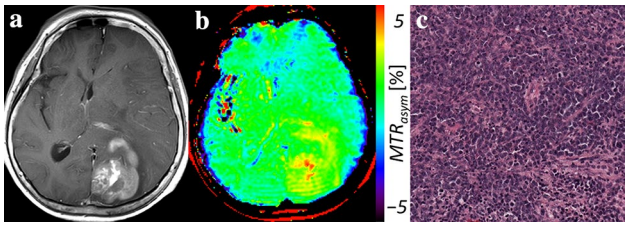


**Fig. 5** Images of a PCNSL. **a** Contrast-enhanced T1-weighted image showing a heterogeneously enhancing mass in the left occipital lobe. **b** APT-weighted image. An intermediate APTWSI (approximately 1–3%) is observable in the enhancing tumor. **c** Hematoxylin and eosin (H&E)-stained section showing densely aggregated cells with a high nucleus–cytoplasm ratio

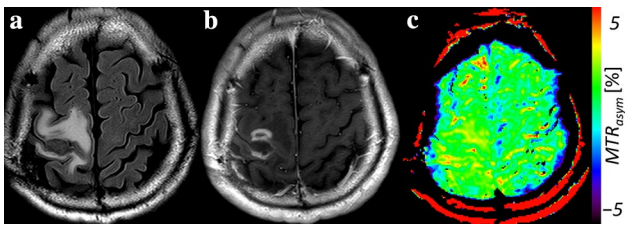


**Fig. 6** Radiation necrosis in a 63-year-old male with postoperative atypical meningioma treated with surgical resection and $\gamma$-knife radiotherapy. **a** FLAIR and **b** contrast-enhanced T1-weighted images obtained 7 months after the completion of radiotherapy, showing an enhancing lesion with surrounding edema in the postoperative region. **c** Corresponding APT-weighted image showing no elevation of APTWSI in the lesion

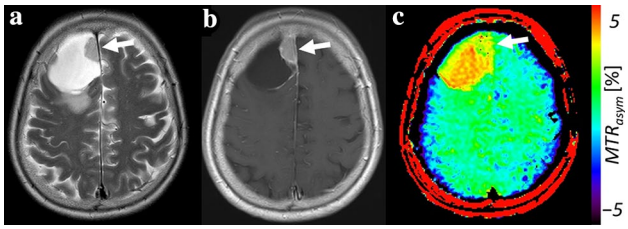


**Fig. 7** Images from a 67-year-old female with a cystic meningioma (grade I) in the right frontal convexity. **a** T2-weighted and **b** contrast-enhanced T1-weighted images, revealing a homogeneous solid component (arrows) and a large cystic component. **c** APT-weighted image. The cystic component shows a high APTWSI, whereas the solid component (arrow) shows a relatively low APTWSI

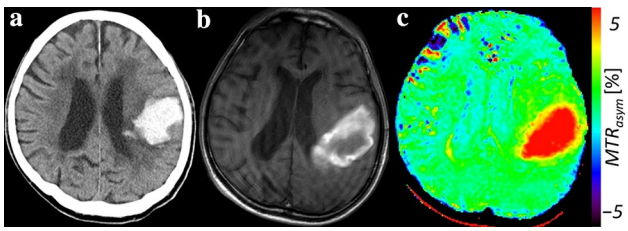


**Fig. 8** Images from a 79-year-old male with an acute hematoma in the left parietal lobe. **a** CT image showing a high-density mass. **b** T1-weighted image. The hematoma shows a heterogeneous signal intensity. **c** Corresponding APT-weighted image, revealing a markedly high APTWSI

## Discrimination between treatment-related changes and viable tumors

Chemoradiation therapy following surgical resection has been regarded as a standard treatment for high-grade gliomas [43]. When an enhancing lesion emerges during a follow-up MR examination in patients with post-treatment gliomas, differentiation between recurrent tumors and treatment-related changes is crucial but often challenging with conventional MR techniques [44]. An animal experiment predicted the potential utility of APT as a biomarker for this differentiation [45], and this utility has been verified in several clinical studies [46–49]. In these studies, recurrent tumors showed significantly higher APTWSIs than treatment-related changes; these high APTWSIs may be related to active proliferation. Figure 6 shows an APT-weighted image of a case of clinically diagnosed radiation necrosis.

## Pitfalls and limitations

Despite previous reports showing the clinical value of APT imaging in the management of brain tumors, the sources of signal contributors in APT imaging is only partially understood. In brain tumor imaging, intracellular cytosolic protein has been the primarily hypothesized source of APT contrast. However, clinical and experimental studies have shown that there may be other sources of contributions to increased APTWSIs.

First, it is known that a high APTWSI is often observed in cysts and cavities filled with protein-containing fluid [50]. Figure 7 shows an example of cystic tumor with a high APTWSI. A high APTWSI in cysts appears to be independent of the malignancy grade. Thus, cystic components have been carefully excluded in previous studies on the evaluation of gliomas [35, 46].

Second, there are several reports of hematoma as a source of high APTWSI [51, 52] (Fig. 8). Blood includes abundant proteins, such as albumin, and peptides. A previous experimental report showed that porcine whole blood samples showed large $MTR_{asym}$ values greater than 10%, peaking at 2.5–3 ppm at 3 T [53]. In an animal study using a rat model, an increased APTWSI was observed in a hyperacute intracranial hemorrhage [51]. In a clinical report, acute hemorrhages showed high APTWSIs even without cellular contributions [51]. High APTWSIs have also been seen in blood flowing in vessels [53]. Recently, very high APTWSIs ($MTR_{asym}$ values of up to 6.9%) have been reported in a

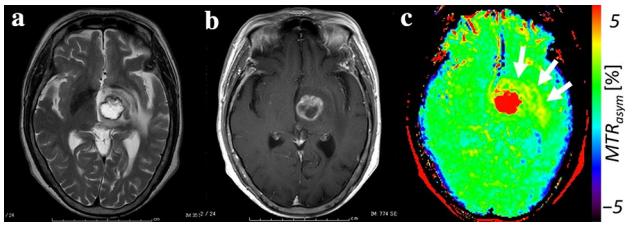


**Fig. 9** Images from a 70-year-old female with a metastatic tumor from lung cancer. **a** T2-weighted and **b** contrast-enhanced T1-weighted images showing a rim-enhancing mass with peritumoral edema in the left thalamus. **c** APT-weighted image showing increased APTWSI in the edematous areas (arrows)

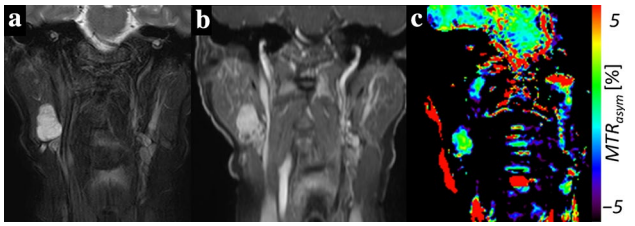


**Fig. 10** Images from a 51-year-old female with a right parotid benign pleomorphic adenoma. **a** Fat-suppressed T2-weighted image. The lobulated mass shows a homogeneous high signal intensity. **b** Avid enhancement following contrast administration. **c** APT-weighted image. The mass shows a low APTWSI of 0.88%

cavernous malformation [54]. Thus, blood in tumor vessels is a potential source of high APTWSIs in hypervascular tumors. Several studies have revealed that edematous brain tissue can show an increased APTWSI. In an early study by Wen et al. [50], it was found that the APTWSI in edematous areas adjacent to the tumor core was significantly higher than that in normal-appearing white matter in the contralateral hemisphere in patients with gliomas. Because glioma cells can invade beyond the tumor core, the increased APTWSI may be attributable to either amides in infiltrating tumor cells or edema. More importantly, Yu et al. [55] have reported that the APTWSI was significantly higher in edematous areas surrounding brain metastases than in normal-appearing white matter. Because edematous areas surrounding a brain metastasis represent vasogenic edema and usually include no tumor cells, this result strongly suggests that edema can be associated with increased APTWSI. This finding was attributed to intravascular proteins and peptides penetrating into the extravascular space through a leaky blood–brain barrier. Figure 9 shows a case of a brain metastasis with an increased APTWSI in the surrounding edema.

Finally, as mentioned earlier, the APTWSI can be affected by the local pH and temperature through alterations in the proton exchange rate. Studies have shown that in many tumor types, the intracellular pH is higher than that in normal brain tissue [56]. Because the amide proton exchange rate is base-catalyzed in the physiological pH range, the exchange rate increases with increasing pH, thus increasing the APT contrast. Nevertheless, the pH has not been considered to be a major source of increased APTWSI in malignant tumors. These should be recognized as possible confounding factors in interpreting APT imaging results.

## Future directions in oncology

Recent studies have suggested the feasibility of APT imaging in extracranial locations where motion- and/or fat-related artifacts and magnetic field inhomogeneities can hamper accurate measurement. Yuan et al. [57] demonstrated the technical feasibility of APT imaging in the head and neck region using a clinical 3 T scanner. A successful example of a head and neck APT image is presented in Fig. 10. The role of APT imaging in differential diagnosis and the prediction of treatment outcomes will be examined in the near future. Recently, APT imaging has been attempted in more challenging parts of the body. Takayama et al. [58] have reported the usefulness of APT imaging in estimating the histological grade of endometrial adenocarcinoma in the uterus. Additional attempts have been made in the breast [59] and lung [60], where more sophisticated imaging techniques for minimizing artifacts such as motion correction and fat signal suppression are needed.

## Conclusion

APT imaging has shown promise in the preoperative grading and prediction of genetic mutation in gliomas, differential diagnosis among brain tumors, and differentiation between treatment-related changes and viable malignant tumors. However, various pathological conditions without intracellular proteins can show increased APTWSIs, and such cases should not be mistaken for malignant tumors. The feasibility of APT imaging in extracranial locations has been recently demonstrated, opening new possibilities to extending its range of application.

**Acknowledgements** This paper was presented at the 103rd annual meeting of the Radiological Society of North America (RSNA) in Chicago, 2017. It received a Certification of Merit for an education exhibit. The authors would like to thank the staff of Kagoshima University Hospital for their support.

**Funding** The authors state that this work has not received any funding.

## Compliance with ethical standards

**Conflict of interest** The authors declare that they have no conflict of interest.

**Ethical statement** This manuscript is a review article and does not contain any studies with human participants or animals performed by any of the authors.

## References


1. Louis DN, Ohgaki H, Wiestler OD, Cavenee WK. WHO classification of tumours of the central nervous system. 4th ed. Lyon: IARC; 2016.
2. Sugahara T, Korogi Y, Kochi M, Ikushima I, Shigematu Y, Hirai T, et al. Usefulness of diffusion-weighted MRI with echo-planar technique in the evaluation of cellularity in gliomas. J Magn Reson Imaging. 1999;9:53–60.
3. Bulakbasi N, Guvenc I, Onguru O, Erdogan E, Tayfun C, Ucoz T. The added value of the apparent diffusion coefficient calculation to magnetic resonance imaging in the differentiation and grading of malignant brain tumors. J Comput Assist Tomogr. 2004;28:735–46.
4. Aronen HJ, Gazit IE, Louis DN, Buchbinder BR, Pardo FS, Weisskoff RM, et al. Cerebral blood volume maps of gliomas: comparison with tumor grade and histologic findings. Radiology. 1994;191:41–51.
5. Sugahara T, Korogi Y, Kochi M, Ikushima I, Hirai T, Okuda T, et al. Correlation of MR imaging-determined cerebral blood volume maps with histologic and angiographic determination of vascularity of gliomas. AJR Am J Roentgenol. 1998;171:1479–86.
6. Ward KM, Aletras AH, Balaban RS. A new class of contrast agents for MRI based on proton chemical exchange dependent saturation transfer (CEST). J Magn Reson. 2000;143:79–87.
7. Zhou J, Payen JF, Wilson DA, Traystman RJ, van Zijl PC. Using the amide proton signals of intracellular proteins and peptides to detect pH effects in MRI. Nat Med. 2003;9:1085–90.
8. Zhang S, Winter P, Wu K, Sherry AD. A novel europium(III)-based MRI contrast agent. J Am Chem Soc. 2001;123:1517–8.
9. Aime S, Delli Castelli D, Terreno E. Highly sensitive MRI chemical exchange saturation transfer agents using liposomes. Angew Chem Int Ed Engl. 2005;44:5513–5.
10. Chan KW, McMahon MT, Kato Y, Liu G, Bulte JW, Bhujwalla ZM, et al. Natural D-glucose as a biodegradable MRI contrast agent for detecting cancer. Magn Reson Med. 2012;68:1764–73.
11. Dagher A, Aletras A, Choyke P, Balaban R. Imaging of urea using chemical exchange-dependent saturation transfer at 1.5 T. J Magn Reson Imaging. 2000;12:745–8.
12. van Zijl PC, Jones CK, Ren J, Malloy CR, Sherry AD. MRI detection of glycogen in vivo by using chemical exchange saturation transfer imaging (glycoCEST). Proc Natl Acad Sci USA. 2007;104:4359–64.
13. Ling W, Regatte RR, Navon G, Jerschow A. Assessment of glycosaminoglycan concentration in vivo by chemical exchange-dependent saturation transfer (gagCEST). Proc Natl Acad Sci USA. 2008;105:2266–70.
14. Haris M, Cai K, Singh A, Hariharan H, Reddy R. In vivo mapping of brain myo-inositol. Neuroimage. 2011;54:2079–85.
15. Cai K, Haris M, Singh A, Kogan F, Greenberg JH, Hariharan H, et al. Magnetic resonance imaging of glutamate. Nat Med. 2012;18:302–6.
16. Haris M, Nanga RP, Singh A, Cai K, Kogan F, Hariharan H, et al. Exchange rates of creatine kinase metabolites: feasibility of imaging creatine by chemical exchange saturation transfer MRI. NMR Biomed. 2012;25:1305–9.
17. Togao O, Hiwatashi A, Keupp J, Yamashita K, Kikuchi K, Yoshiura T, et al. Amide proton transfer imaging of diffuse gliomas: effect of saturation pulse length in parallel transmission-based technique. PLoS One. 2016;11:e0155925 **(Accessed May 10, 2018)**.
18. Keupp J, Eggers H. (2012) Intrinsic field homogeneity correction in fast spin echo based amide proton transfer MRI. In: Proceedings of the 20th annual meeting of ISMRM, Melbourne, Australia, 2012. Abstract 4185.
19. Dixon WT, Hancu I, Ratnakar SJ, Sherry AD, Lenkinski RE, Alsop DC. A multislice gradient echo pulse sequence for CEST imaging. Magn Reson Med. 2010;63:253–6.
20. Ng MC, Hua J, Hu Y, Luk KD, Lam EY. Magnetization transfer (MT) asymmetry around the water resonance in human cervical spinal cord. J Magn Reson Imaging. 2009;29:523–8.
21. Keupp J, Doneva M, Senegas J, Hey S, Eggers H. (2014) 3D fast spin-echo amide proton transfer MR with intrinsic field homogeneity correction for neuro-oncology applications. In: Proceedings of the 22nd annual meeting of ISMRM, Milan, Italy, 2014. Abstract 3150.
22. Jones CK, Polders D, Hua J, Zhu H, Hoogduin HJ, Zhou J, et al. In vivo three-dimensional whole-brain pulsed steady-state chemical exchange saturation transfer at 7 T. Magn Reson Med. 2012;67:1579–89.
23. Kim M, Gillen J, Landman B, Zhou JY, van Zijl PC. Water saturation shift referencing (WASSR) for chemical exchange saturation transfer (CEST) experiments. Magn Reson Med. 2009;61:1441–50.
24. Sun PZ, Farrar CT, Sorensen AG. Correction for artifacts induced by B0 and B1 field inhomogeneities in pH-sensitive chemical exchange saturation transfer (CEST) imaging. Magn Reson Med. 2007;58:1207–15.
25. Bryant RG. The dynamics of water–protein interactions. Annu Rev Biophys Biomol Struct. 1996;25:29–53.
26. van Zijl PC, Zhou J, Mori N, Payen JF, Wilson D, Mori S. Mechanism of magnetization transfer during on-resonance water saturation: a new approach to detect mobile proteins, peptides, and lipids. Magn Reson Med. 2003;49:440–9.
27. van Zijl PC, Yadav NN. Chemical exchange saturation transfer (CEST): what is in a name and what isn't? Magn Reson Med. 2011;65:927–48.
28. Scheidegger R, Vinogradov E, Alsop DC. Amide proton transfer imaging with improved robustness to magnetic field inhomogeneity and magnetization transfer asymmetry using saturation with frequency alternating RF irradiation. Magn Reson Med. 2011;66:1275–85.
29. Lee JS, Regatte RR, Jerschow A. Isolating chemical exchange saturation transfer contrast from magnetization transfer asymmetry under two-frequency rf irradiation. J Magn Reson. 2012;215:56–63.
30. Zhang J, Zhu W, Tain R, Zhou XJ, Cai K. Improved differentiation of low-grade and high-grade gliomas and detection of tumor proliferation using APT contrast fitted from Z-spectrum. Mol Imaging Biol. 2018;20:623–31.
31. Yan K, Fu Z, Yang C, Zhang K, Jiang S, Lee DH, et al. Assessing amide proton transfer (APT) MRI contrast origins in 9 L gliosarcoma in the rat brain using proteomic analysis. Mol Imaging Biol. 2015;17:479–87.
32. Li J, Zhuang Z, Okamoto H, Vortmeyer AO, Park DM, Furuta M, et al. Proteomic profiling distinguishes astrocytomas and identifies differential tumor markers. Neurology. 2006;66:733–6.
33. Clarke J, Butowski N, Chang S. Recent advances in therapy for glioblastoma. Arch Neurol. 2010;67:279–83.
34. Zhou J, Blakeley JO, Hua J, Kim M, Laterra J, Pomper MG, et al. Practical data acquisition method for human brain tumor amide proton transfer (APT) imaging. Magn Reson Med. 2008;60:842–9.
35. Togao O, Yoshiura T, Keupp J, Hiwatashi A, Yamashita K, Kikuchi K, et al. Amide proton transfer imaging of adult diffuse

gliomas: correlation with histopathological grades. Neuro Oncol. 2014;16:441–8.
36. Togao O, Hiwatashi A, Yamashita K, Kikuchi K, Keupp J, Yoshimoto K, et al. Grading diffuse gliomas without intense contrast enhancement by amide proton transfer MR imaging: comparisons with diffusion- and perfusion-weighted imaging. Eur Radiol. 2017;27:578–88.
37. Choi YS, Ahn SS, Lee SK, Chang JH, Kang SG, Kim SH, et al. Amide proton transfer imaging to discriminate between low- and high-grade gliomas: added value to apparent diffusion coefficient and relative cerebral blood volume. Eur Radiol. 2017;27:3181–9.
38. Sakata A, Fushimi Y, Okada T, Arakawa Y, Kunieda T, Minamiguchi S, et al. Diagnostic performance between contrast enhancement, proton MR spectroscopy, and amide proton transfer imaging in patients with brain tumors. J Magn Reson Imaging. 2017;46:732–9.
39. Eckel-Passow JE, Lachance DH, Molinaro AM, Walsh KM, Decker PA, Sicotte H, et al. Glioma groups based on 1p/19q, IDH, and TERT promoter mutations in tumors. N Engl J Med. 2015;372:2499–508.
40. The Cancer Genome Atlas Research Network. Comprehensive, integrative genomic analysis of diffuse lower-grade gliomas. N Engl J Med. 2015;372:2481–98.
41. Jiang S, Zou T, Eberhart CG, Villalobos MAV, Heo HY, Zhang Y, et al. Predicting IDH mutation status in grade II gliomas using amide proton transfer-weighted (APTw) MRI. Magn Reson Med. 2017;78:1100–9.
42. Jiang S, Yu H, Wang X, Lu S, Li Y, Feng L, et al. Molecular MRI differentiation between primary central nervous system lymphomas and high-grade gliomas using endogenous protein-based amide proton transfer MR imaging at 3 Tesla. Eur Radiol. 2016;26:64–71.
43. Stupp R, Mason WP, van den Bent MJ, Weller M, Fisher B, Taphoorn MJ, et al. Radiotherapy plus concomitant and adjuvant temozolomide for glioblastoma. N Engl J Med. 2005;352:987–96.
44. Kanda T, Wakabayashi Y, Zeng F, Ueno Y, Sofue K, Maeda T, et al. Imaging findings in radiation therapy complications of the central nervous system. Jpn J Radiol. 2018. https://doi.org/10.1007/s11604-018-0759-7.
45. Zhou J, Tryggestad E, Wen Z, Lal B, Zhou T, Grossman R, et al. Differentiation between glioma and radiation necrosis using molecular magnetic resonance imaging of endogenous proteins and peptides. Nat Med. 2011;17:130–4.
46. Park JE, Kim HS, Park KJ, Kim SJ, Kim JH, Smith SA. Pre- and posttreatment glioma: comparison of amide proton transfer imaging with MR spectroscopy for biomarkers of tumor proliferation. Radiology. 2016;278:514–23.
47. Park KJ, Kim HS, Park JE, Shim WH, Kim SJ, Smith SA. Added value of amide proton transfer imaging to conventional and perfusion MR imaging for evaluating the treatment response of newly diagnosed glioblastoma. Eur Radiol. 2016;26:4390–403.
48. Mehrabian H, Desmond KL, Soliman H, Sahgal A, Stanisz GJ. Differentiation between radiation necrosis and tumor progression using chemical exchange saturation transfer. Clin Cancer Res. 2017;23:3667–75.
49. Park JE, Lee JY, Kim HS, Oh JY, Jung SC, Kim SJ, et al. Amide proton transfer imaging seems to provide higher diagnostic performance in post-treatment high-grade gliomas than methionine positron emission tomography. Eur Radiol. 2018;28:3285–95.
50. Wen Z, Hu S, Huang F, Wang X, Guo L, Quan X, et al. MR imaging of high-grade brain tumors using endogenous protein and peptide-based contrast. Neuroimage. 2010;51:616–22.
51. Wang M, Hong X, Chang CF, Li Q, Ma B, Zhang H, et al. Simultaneous detection and separation of hyperacute intracerebral hemorrhage and cerebral ischemia using amide proton transfer MRI. Magn Reson Med. 2015;74:42–50.
52. Jeong HK, Han K, Zhou J, Zhao Y, Choi YS, Lee SK, et al. Characterizing amide proton transfer imaging in haemorrhage brain lesions using 3 T MRI. Eur Radiol. 2017;27:1577–84.
53. Zheng S, van der Bom IM, Zu Z, Lin G, Zhao Y, Gounis MJ. Chemical exchange saturation transfer effect in blood. Magn Reson Med. 2014;71:1082–92.
54. Bohara M, Kamimura K, Nakajo M, Yoneyama T, Yoshiura T. Amide proton transfer imaging of cavernous malformation in the cavernous sinus. Magn Reson Med Sci. 2018. https://doi.org/10.2463/mrms.ci.2017-0160.
55. Yu H, Lou H, Zou T, Wang X, Jiang S, Huang Z, et al. Applying protein-based amide proton transfer MR imaging to distinguish solitary brain metastases from glioblastoma. Eur Radiol. 2017;27:4516–24.
56. Ross BD, Higgins RJ, Boggan JE, Knittel B, Garwood M. 31P NMR spectroscopy of the in vivo metabolism of an intracerebral glioma in the rat. Magn Reson Med. 1988;6:403–17.
57. Yuan J, Chen S, King AD, Zhou J, Bhatia KS, Zhang Q, et al. Amide proton transfer-weighted imaging of the head and neck at 3 T: a feasibility study on healthy human subjects and patients with head and neck cancer. NMR Biomed. 2014;27:1239–47.
58. Takayama Y, Nishie A, Togao O, Asayama Y, Ishigami K, Ushijima Y, et al. Amide proton transfer MR imaging of endometrioid endometrial adenocarcinoma: association with histologic grade. Radiology. 2018;286:909–17.
59. Klomp DW, Dula AN, Arlinghaus LR, Italiaander M, Dortch RD, Zu Z, et al. Amide proton transfer imaging of the human breast at 7T: development and reproducibility. NMR Biomed. 2013;26:1271–7.
60. Ohno Y, Yui M, Koyama H, Yoshikawa T, Seki S, Ueno Y, et al. Chemical exchange saturation transfer MR imaging: preliminary results for differentiation of malignant and benign thoracic lesions. Radiology. 2016;279:578–89.